RESEARCH

Optimization analysis of gate width for detecting atmospheric turbulence with differential image motion LiDAR

Hui Zhou[1,2,3,4] · Chenbo Xie[1,3] · Yalin Hu[1,2,3] · Fahua Shen[4] · Kunming Xing[1,3] · Yingjian Wang[1,3] · Bangxin Wang[1,3]

Abstract
Through theoretical calculations and field experiments, the setting of gate width in distance gating technology has been optimized in DIM LiDAR. The mathematical relationship between gate width and detection distance has been derived. The relationship curves between gate width and image signal-to-noise ratio(SNR), as well as gate width and atmospheric refractive index structure constant C_n^2 were obtained. The results indicate that at a constant detection distance, there is a gradual increase in the SNR of the image with increasing gate width, followed by a saturation point. The higher the SNR, the closer the inverted C_n^2 is to the ultrasonic anemometer. Meanwhile, if the SNR is similar, the inverted C_n^2 is similar. Finally, the appropriate gate width for this system is given.

1 Introduction

In the field of atmospheric optics, turbulence is a random change in atmospheric refractive index caused by local temperature and pressure variations. When laser is transmitted in turbulent atmosphere, due to the fluctuation of atmospheric refractive index, the laser wavefront is distorted and the coherence of the laser is disrupted. Therefore, phenomena such as random drift, expansion, distortion, and scintillation of the transmitted beam are called atmospheric turbulence effects [1, 2]. According to Kolmogorov and Tatarski's turbulence theory, turbulence intensity is described by the

atmospheric refractive index structure constant C_n^2 [3, 4]. The variation characteristics of C_n^2 in local areas can be obtained through long-term measurements, providing a basis for studying the effects of laser atmospheric transmission. Among many methods for measuring C_n^2, optical measurement is the most commonly [5–7]. Among them, Differential Image Motion (DIM) LiDAR can measure atmospheric turbulence values at different detection distances. Pulse laser and range gating technology are combined in DIM LiDAR. Therefore, the imaging spot of laser guide stars at different positions can be detected. Turbulence intensity is inverted by calculating the differential motion variance of the imaging spot.

Laser guide stars are based on the principle of Rayleigh beacons. The Rayleigh beacon is formed by the atmospheric

---

Chenbo Xie, Yalin Hu, Fahua Shen, Kunming Xing, Yingjian Wang and Bangxin Wang contributed equally to this work.

✉ Chenbo Xie
   cbxie@aiofm.ac.cn

   Hui Zhou
   zhouhuiedu@163.com

   Yalin Hu
   hylheihei@mail.ustc.edu.cn

   Fahua Shen
   sfh81914@163.com

   Kunming Xing
   kunmingx@mail.ustc.edu.cn

   Yingjian Wang
   wyj@aiofm.ac.cn

   Bangxin Wang
   bxwang@aiofm.ac.cn

1   Key Laboratory of Atmospheric Optics Anhui Institute of Optics and Fine Mechanics, Hefei Institutes of Physical Science, Chinese Academy of Sciences, Hefei 230031, Anhui, People's Republic of China

2   University of Science and Technology of China, Hefei 230026, People's Republic of China

3   Advanced Laser Technology Laboratory of Anhui Province, Hefei 230027, People's Republic of China

4   Department of Physics and Electronic Engineering, Yancheng Teachers University, Yancheng 224002, Jiangsu, People's Republic of China

backscatter of a focused laser beam emitted by the lidar emission system at the focal point. It is the beacon of the LiDAR receiving system [8]. To measure turbulence values at different distances, it is necessary to receive backscattered signals from different positions. So, in the DIM LiDAR, distance gating technology was used to adjust the exposure delay and gate width of the Image Intensifier (ICCD) accordingly. Among them, the sampling thickness of the scattering position is determined by the gate width. The detection accuracy will be reduced due to unreasonable gate width. On the one hand, insufficient detection energy is caused by a too small sampling thickness; On the other hand, the formation of diffuse spots on the focal plane is caused by excessive sampling thickness. Therefore, it is necessary to control the gate width according to the system detection requirements.

Due to the time selective nature of distance gating technology, both distance and intensity information of the target scenery can be obtained simultaneously. It has been widely applied in fields such as target recognition, underwater vision, and 3D imaging. In 2009, Jian et al. [9] studied the relationship between time gating accuracy, time interval, and imaging quality. When the gating signal is appropriate, the influence of water scattering light noise on the distance gated laser underwater imaging system is reduced, and high-quality images are obtained. In 2013, Ge et al. [10] simulated that when the gate width is greater than the laser pulse width, the water backscattered light noise energy received by ICCD is larger and the signal-to-noise ratio(SNR) is lower. When the gate width is close to the laser pulse width at the same position, the SNR is highest. In 2015, Xu et al. [11] analyzed the impact of delay accuracy on imaging quality, and proposed the idea of precise measurement replacing precise time control. The imaging accuracy is achieved at the centimeter level in the gated slicing laser imaging trigger control system. In 2015, Rui et al. [12] analyzed the SNR of images under different gate widths. The relationship between gate width and image SNR is obtained. In laser range-gated imaging, when the gate width is increased, the SNR is reduced. In 2016, Xiaobo et al. [13] combined the principle of distance gated imaging to estimate the received energy and noise of the detector. By establishing an imaging parameter model, it is concluded that a stable and uniform target image must be obtained by comprehensively considering the effects of pulse width, detector width bandwidth, and gating distance. In 2023, Qianqian et al. [14] investigated the effects of experimental conditions such as laser output power, ICCD gate width, and distance from laser focus to sample surface on LIBS signal intensity and SNR. Among them, when the gate width is increased, the spectral signal intensity is increased. When the gate width is 5 µs, the signal strength and SNR are the highest. Continuing to increase the gate width, there was no significant change in signal strength, and SNR was significantly reduced. The above

research indicates that in order to achieve optimal system performance, the setting of operating parameters in distance gating technology needs to be balanced. Furthermore, it can be adaptively operated in different scenarios.

In this study, the specific requirements for distance gating gate width were analyzed based on the principle of detecting turbulence at different positions using DIM LiDAR. Field experiments were conducted using DIM LiDAR, and the effects of spot images obtained under different gate widths were analyzed. By comparing the inversion results of C_n^2 obtained from spot images with those obtained from ultrasonic anemometers, the relationship between distance gate width, SNR of spot images, and C_n^2 was explored. Meanwhile, further experiments were conducted to provide suitable gate widths for turbulence detection at different positions.

2 Theory

2.1 Principle of turbulence intensity detection with DIM LiDAR

The star light source in DIMM (Differential Image Motion Monitor) has been replaced by laser in DIM LiDAR. Imaging of Laser Guided Stars (LGS) is achieved through spatially separated sub-pupil telescopes. Due to the random fluctuations in the wavefront arrival angle of each pupil, image movement is generated on the focal plane. Therefore, the intensity of atmospheric turbulence can be inverted based on the moving σ^2 of the two images. The specific process is shown in Fig. 1.

By using distance gating technology, the backscattered signal near the measured distance L_i is received by two sub-apertures of the DIM LiDAR. This signal appears as two light spots in the ICCD. An image set will be collected at this distance. To obtain the centroids of the two light spots in each image, three steps are required: denoising, segmentation, and centroid extraction. Then, the jitter variance σ^2 is calculated based on this. According to literature [7], the relationship between σ^2 and the atmospheric coherence length r_0 is described as Eq. 1. Also, the horizontal C_n^2 can be inverted from r_0 according to Eq. 2.

$$r_0 = \left\{ \frac{2f^2[0.358(\lambda/D)^{1/3} - 0.242(\lambda/d)^{1/3}]\lambda^{5/3}}{\sigma^2} \right\}^{3/5} \tag{1}$$

$$C_n^2 = \left[(r_0/1.68)^{-5/3} \right] / L_i k^2 \tag{2}$$

where f is focal length, λ is laser wavelength, D is distance mirror pupil diameter, d is distance between the pupil centers of a telescope mirror, and k is wave number.

Fig. 1 The principle of detecting turbulence using DIM LiDAR
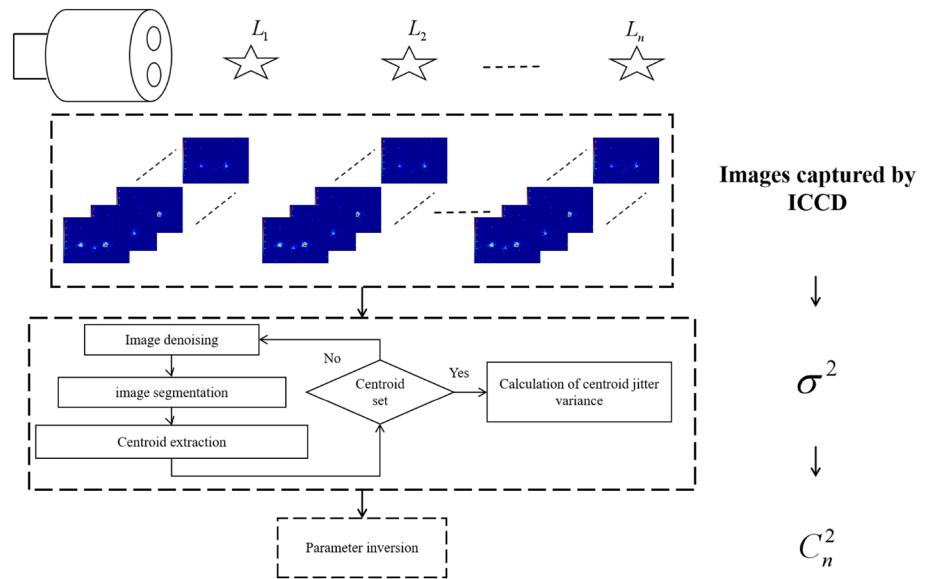
Therefore, it can be inferred that the relationship between σ^2 and C_n^2 can be described as Eq. 3

$$C_n^2 = \frac{\sigma^2}{0.843(f\lambda k)^2 L_i(0.358D^{-1/3} - 0.242d^{-1/3})} \quad (3)$$

Based on the assumption that the atmosphere is uniform in the horizontal direction, C_n^2 remains constant in that direction. Meanwhile, as indicated by Eq. 3, only L_i and σ^2 are variable, while the other variables are system parameters. Therefore, when C_n^2 and L_i are not changed, σ^2 remains unchanged. In the previous text, σ^2 is the inversion of the image set collected by ICCD. Therefore, to ensure consistent inversion results, good image quality is required. The image obtained by DIM LiDAR depends on the parameters in distance gating technology. However, this article focuses on the setting of the gate width for ICCD in the context of distance gating technology.

2.2 Principle of distance gating technology

The principle of distance gating technology applied in DIM LiDAR is shown in Fig. 2. The specific implementation steps are as follows:

Step1: The laser pulse is emitted by the laser at a certain repetition rate, and the trigger signal is synchronously generated.

Step2: According to the above trigger signals and Eq. 4, delay trigger signals corresponding to different L_i are generated. So, based on the delayed trigger signal, the backscatter signals of different L_i are collected by ICCD.

$$t_i = CL_i/2, \quad (4)$$

where t_i is the delay corresponding to different L_i.

Step3: The ICCD acquisition is triggered by the rising edge of the delayed signal. By setting the gate width t_p, the length of the collected light column, i.e. the sampling thickness Δz_i is determined.

$$\Delta z = ct_p/2 \quad (5)$$

According to literature [8], if the sampling thickness exceeds the depth of field, then the accuracy of detection will be affected. It can be seen that the backscattered signal near the detection point should be collected. The depth of field of an optical system is represented by Eq. 6.

$$\Delta = \frac{4ap^2\varepsilon}{4a^2 - p^2\varepsilon^2} \quad (6)$$

where a is the entering pupil radius, and p is the distance between the object surface and the center of the entering pupil, ε is the maximum resolution angle.

The calculation equation for ε is described as:

$$\varepsilon = \frac{1.22\lambda}{d} \quad (7)$$

As mentioned above, it can be inferred that $\Delta z \leq \Delta$. The gate width t_p should be set in accordance with Eq. 8.

$$t_p \leq \frac{2.44\lambda a L_i^2 d}{(a^2 d^2 - 0.37 L_i^2 \lambda^2)c} \quad (8)$$

It can be seen that the limit of t_p is determined by the wavelength of the laser λ, detection position L_i, entrance pupil radius a, and the diameter of the receiving telescope pupil d. Excluding system parameters, only L_i is a variable. Therefore, it is necessary to explore the specific relationship between the detection positions L_i and t_p.

Fig. 2 The principle of distance gating technology
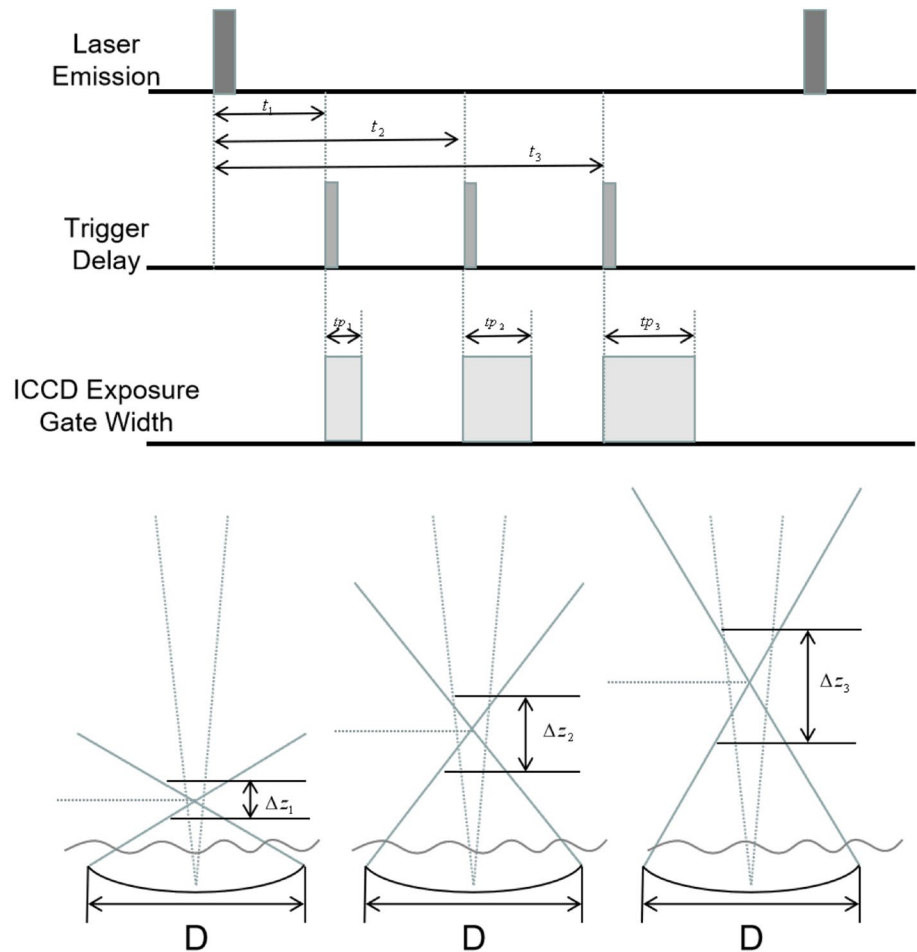
3 System introduction

The necessity of setting the gate width t_p reasonably when detecting turbulence using DIM LiDAR under certain system parameter conditions has been verified from an experimental perspective in this study. A schematic diagram depicting the DIM LiDAR system is presented in Fig. 3. The system can be primarily categorized into three parts, namely laser emission, signal reception, and data acquisition and processing. Firstly, the emission is achieved using a 532 nm laser. Then, the echo light signals are received using the telescope's pupil for signal reception. Since this study is probed along a horizontal path and the location is in the bottom atmosphere, the Mie scattering and Rayleigh scattering signals are included in the received echo signals. Finally, the spot image is captured by an ICCD
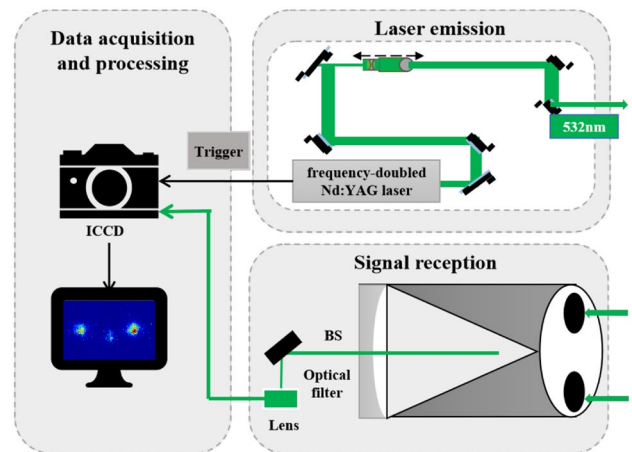

Fig. 3 System for DIM LiDAR

camera, and C_n^2 is inverted in the computer. Table 1 shows the system parameters of DIM LiDAR.

Parameters	Value
Laser	Frequency-doubled Nd:YAG laser
Wavelength	532 nm
Pulse energy	100 mJ
Pulse width	5–9 ns
Impulse frequency	100 Hz
Telescope	Schmidt–Cassegrain type
Telescope focal length	5 m
Telescope main mirror diameter	400 mm
Distance between the pupil centers of a telescope mirror	250 mm
Distance mirror pupil diameter	120 mm
Optical filter bandwidth	0.3 nm
Camera	Intensified CCD (ICCD)
Camera Resolution	1024×768p
Camera pixel size	8 μm
Camera acquisition frequency	20 fps
Measurement direction	Horizontal

4 Experimental analysis

4.1 Theoretical calculations

In accordance with the principle of detecting turbulence using DIM LiDAR, the setting of the distance gate width should be based on Eq. 8. The relationship between L_i and the maximum t_p is simulated, and a corresponding curve is provided. When L_i is within the range of 500 m to 10 km, the
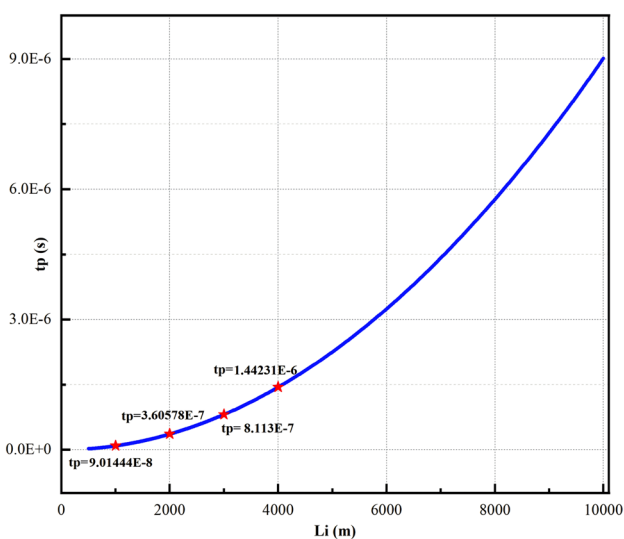

Fig. 4 The maximum gate width corresponding to the detection distance

maximum value of t_p is shown in Fig. 4. It can be seen that as the detection distance L_i is increased, the maximum value of the gate width t_p is also increased. The maximum gate width t_p for different detection distances is given. The maximum t_p for L_i at 1 km, 2 km, 3 km, and 4 km are 90.14 ns, 360.58 ns, 811.3 ns, and 1442 ns, respectively. Moreover, according to the application principle of distance gating technology in DIM LiDAR, it is known that if the t_p is too small, the detection energy is insufficient. Therefore, t_p should be set reasonably.

4.2 Analysis of day and night detection experiments of DIM LiDAR

According to the calculation results in 4.1, corresponding experimental measurements were conducted using DIM LiDAR in the Shushan area of Hefei in December 2023. The purpose of this experiment is to analyze the specific effects of different gate widths at different detection positions. The experiment was conducted during both day and night under clear weather conditions, with a two-hour time interval. Detection positions L_i were set at intervals of 1 km, 2 km, 3 km, and 4 km. Meanwhile, at the same height, an ultrasonic anemometer was placed 1 km away from the exit laser point to measure the C_n^2. Therefore, the C_n^2 inverted by DIM LiDAR can be compared with it.

The t_i and t_p corresponding to different L_i are shown in Table 2. 400 images were collected for each parameter. The image is colored, with a size of 1024×768 and a depth of 16 bits.

4.2.1 Analysis of spot images

A total of 57,600 images were collected in this experiment. To better demonstrate the impact of gate width on image quality, other factors such as background noise should be excluded. Therefore, the night spot image with low background noise was selected for display, as shown in Fig. 5a–c are the spot images with values of 30ns, 70ns, and 90ns for t_p when L_i =1 km, respectively. Figure 5d–f are the spot images with values of 120 ns, 240 ns, and 360ns for t_p at L_i =2 km, respectively. Figure 5g–i are the spot images with values of 400 ns,

Table 2 Setting of t_i and t_p at different L_i

L_i (km)	t_i (rmus)	t_p (ns)	L_i (km)	t_i (rmus)	t_p (ns)
1	6.7	30	3	20.1	400
		70			600
		90			800
		120			800
2	13.4	240	4	26.7	1000
		360			1400

Fig. 5 At 20:00, the comparison of the spot images acquired by the DIM LiDAR with different t_p at different L_i. **a–c** t_p = 30 ns, 70 ns, and 90 ns when L_i = 1 km, respectively; **d–f** t_p =120 ns, 240 ns and 360 ns when L_i = 2 km, respectively; **g–i** t_p = 400 ns, 600 ns and 800 ns when L_i = 3 km, respectively; **j** and **k** t_p = 800 ns, 1000ns and 1400 ns when L_i = 4 km, respectively
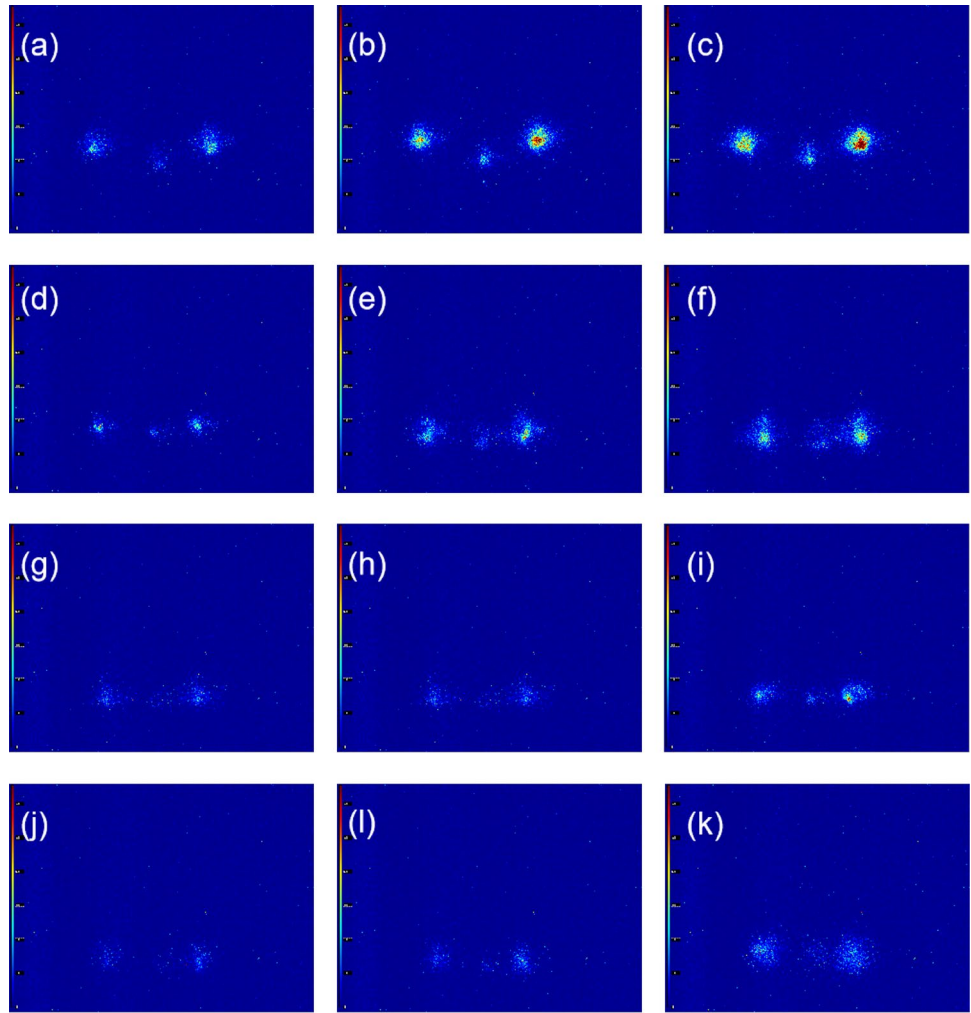
600 ns, and 800ns for t_p at L_i =3 km, respectively. Figure 5j and k are the spot images with values of 800 ns, 1000 ns, and 1400 ns for t_p when L_i =4 km, respectively.

The evaluation of images is usually divided into two types, namely subjective evaluation and objective evaluation. Subjectively, it can be seen that horizontally, when L_i is fixed and t_p is increased, the brightness of the light spot in the image is increased; Vertically, when L_i is increased, the brightness of the spot in the image is decreased. According to Sect. 2.1, the image captured by ICCD needs to be processed to obtain the centroid of the spot, and then the turbulence intensity is inverted based on the variance of centroid jitter. If the image quality is poor, the centroid of the spot will be difficult to accurately obtain, and the inversion of C_n^2 will be affected. Objectively, as there is no original image available as a reference for the images captured by ICCD, no reference image evaluation index such as SNR is selected.

$$SNR = \frac{P_{signal}}{P_{noise}} \tag{9}$$

where P_{signal} and $Pnoise$ are the power of the effective signal part (spot area) in the image and the power of other parts in the image, respectively.

According to Eq. 10, the effective signal $s(x, y)$ and noise signal $n(x, y)$ in the image can be distinguished.

$$\begin{cases} s(x,y) = f(x,y), f(x,y) \geq T \\ n(x,y) = f(x,y), f(x,y) < T \end{cases} \tag{10}$$

where T is the threshold. In this study, the average brightness value of the four corners of the image was used as T.

According to reference [10], the ratio of the mean of the effective signal to the standard deviation of the noisy signal is SNR. Described as Eq. 11:

$$SNR = \frac{\frac{1}{N_s} \sum s(x, y)}{\sqrt{\frac{1}{N_n} \sum \left[n(x, y) - \frac{1}{N_n} \sum n(x, y) \right]^2}} \tag{11}$$

where N_s is the number of effective signal pixels, and N_n is the number of noise signal pixels.

Fig. 6 The SNR of spot images with different t_p at different L_i. **a** $L_i = 1$ km, **b** $L_i = 2$ km, **c** $L_i = 3$ km and **d** $L_i = 4$ km
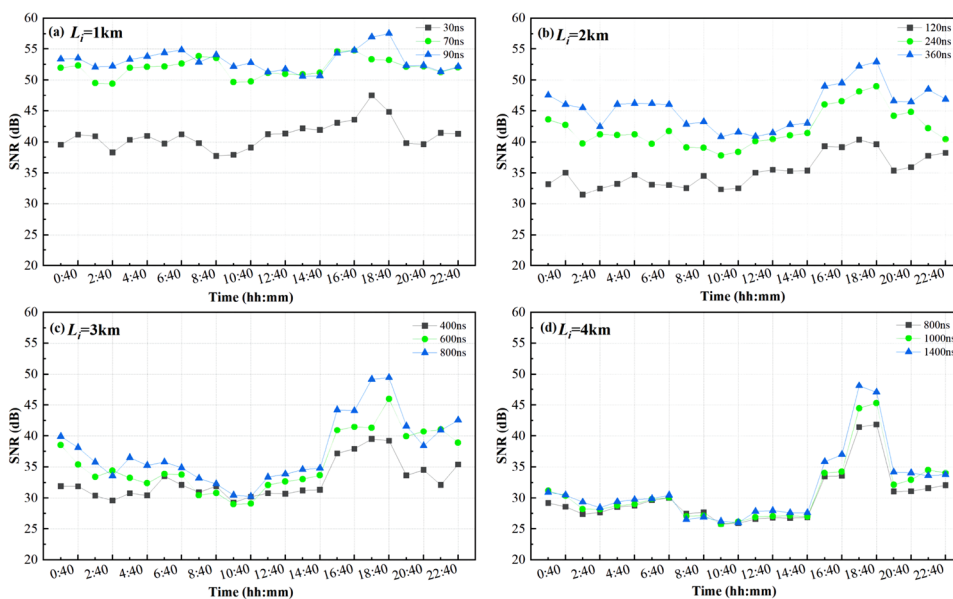

4.2.2 Analysis of inversion results

Due to the fact that C_n^2 is a constant value in the horizontal direction, the profile of C_n^2 that varies over time should theoretically be consistent for different L_i. The comparison of C_n^2 retrieved by DIM LiDAR and the ultrasonic anemometer at different L_i and t_p is shown in Fig. 7.

In order to compare the trend between the inverted C_n^2 curves of DIM LiDAR and ultrasonic anemometer, the cosine similarity between the curves was calculated. Also, in order to compare the values between the inverted C_n^2 curves of DIM LiDAR and ultrasonic anemometer, the mean absolute error (MAE) between the curves was calculated. The results are shown in Table 4.

Table 4 shows that the cosine similarity between the inverted C_n^2 curves of DIM LiDAR and ultrasonic anemometer is basically greater than 0.7. It can be seen that the trend of C_n^2 inverted by DIM LiDAR and ultrasonic anemometer is generally consistent. Among them, when $L_i=1$ km, the curve jitter is maximum. It is more likely to reflect the changes in C_n^2, which is speculated to be related to its larger SNR. Meanwhile, According to Table 4, MAE is maximum when t_p is minimum at the same L_i. It can be seen that the smaller the t_p, the more deviated the curve of C_n^2 obtained by the DIM LiDAR from the ultrasonic anemometer.

According to the experimental analysis, it can be concluded that the SNR of images collected at different t_p values is different when L_i remains constant. And the specific trend of the inverted C_n^2 curve is different. Meanwhile, when L_i is constant, the greater the similarity between the SNR curves, the greater the similarity in the C_n^2 results. For example, when $L_i=1$ km, if the SNR curves of 70 ns and 90 ns

Table 3 Average all-day SNR of different t_p at different L_i

L_i (km)	t_p (ns)	SNR (dB)	L_i (km)	t_p (ns)	SNR (dB)
	30	41.0233		400	32.7756
1	70	51.9403	3	600	35.6681
	90	53.1442		800	37.6211
	120	35.2194		800	30.0026
2	240	42.070	4	1000	30.9010
	360	45.5981		1400	31.6312

Accordingly, the mean SNR of the image set at different times and parameters is calculated, as shown in Fig. 6. Overall, when L_i is increased, SNR will be decreased. And L_i was increased by 1 km, while SNR was reduced by about 5dB. Furthermore, the curve is smoother with a smaller L_i, while it exhibits greater jitter with a larger L_i. It indicates that when the detection distance is far, the SNR of the image is more affected by the detection time. Meanwhile, a common feature is observed in each curve, where the highest SNR of the images is recorded between 16:40 and 18:40.

Additionally, the statistics of the mean SNR for each curve are shown in Table 3. When t_p is increased, SNR will be increased at different times. But the increment of SNR will be affected by the value of L_i. If L_i is shorter, the SNR is more significantly affected by the increase in t_p, and vice versa.

Therefore, both subjective and objective evaluations indicate that image quality is influenced by the setting of gate width at different detection distances.

Fig. 7 Inversion comparison of C_n^2 with different t_p at different L_i, **a** L_i = 1 km, **b** L_i = 2 km, **c** L_i = 3 km and **d** L_i = 4 km
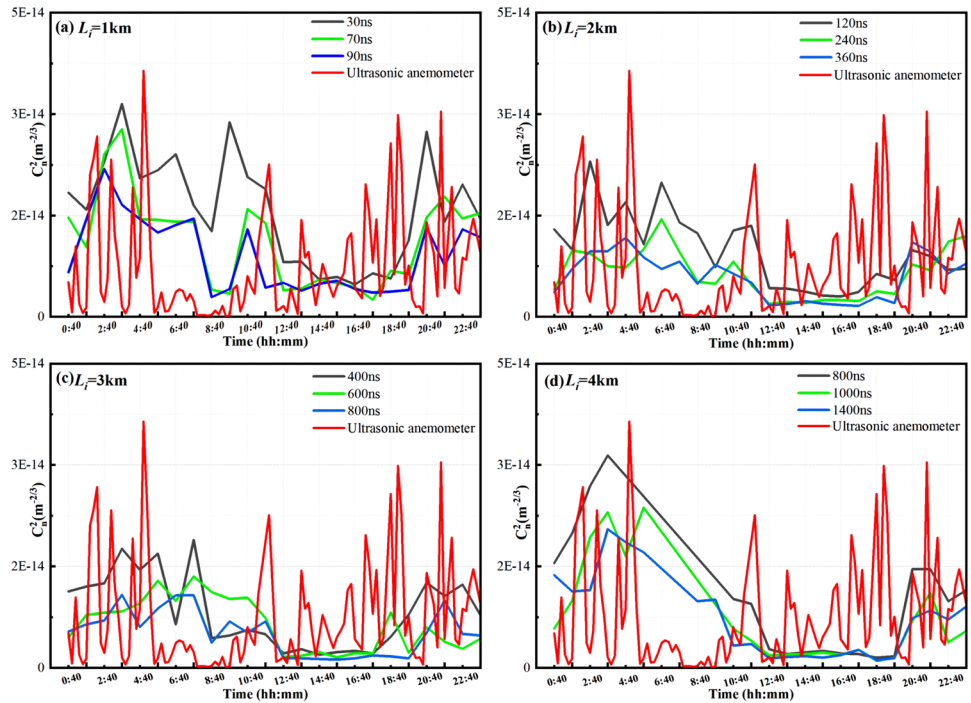

Table 4 Comparison of C_n^2 curves inverted by DIM LiDAR and ultrasonic anemometer with different t_p at different L_i

L_i (km)	t_p (ns)	Cosine similarity	MAE (m$^{-2/3}$)	L_i (km)	t_p (ns)	Cosine similarity	MAE (m$^{-2/3}$)
	30	0.7457	9.87E-15		400	0.6778	6.09E-15
1	70	0.8229	6.45E-15	3	600	0.7353	5.45E-15
	90	0.7865	5.46E-15		800	0.7175	5.39E-15
	120	0.7444	6.59E-15		800	0.7151	7.57E-15
2	240	0.7561	5.24E-15	4	1000	0.7286	5.73E-15
	360	0.7625	5.34E-15		1400	0.7130	6.14E-15

are similar, then the C_n^2 curve is also similar. And the same conclusion is presented in other L_i.

4.3 Optimization experiment of gating gate width

Due to the limitation of maximum gate width and the correlation between t_p, SNR and C_n^2, it is speculated that there are different effective t_p for different L_i, which can be set based on the SNR of the collected image. Therefore, through experimental methods, the reasonable setting of t_p at L_i =1, 2, 3, and 4 km was studied. Clear weather is selected for 4 h: morning, afternoon, evening, and night. When L_i =1, 2, 3, and 4 km, 20 photos were taken for each t_p and their average SNR was calculated. The results are shown in Fig. 8.

Overall, the SNR of all 16 curves is increased with the increase of t_p and no further escalation is observed after a certain juncture. And the growth rate in the first half of the curve is large, but the growth trend in the second half is gentle, especially when L_i =1 km, 2 km.

From the perspective of detection time, the curve can be divided into three categories: nighttime, morning and afternoon, and evening.

1. The black curve is obtained from evening detection. It can be seen that under the four detection distances, the trend of SNR increasing with t_p is the highest compared to other times. It may be that on the one hand the turbulence is weak at the moment of sunset transition, and on the other hand the detection direction is far from the direct sunlight and the background light noise is low.

2. The red and blue curves are obtained from the morning and afternoon detections, respectively. It can be seen that the two curves are affected by the detection distance. When L_i =1 km and 2 km, the curve growth trend is relatively large, while when L_i =3 km and 4 km, the curve growth trend is slow. And compared to the other two curves, the SNR value is smaller.

Fig. 8 The SNR of spot images with different t_p at different L_i. **a** L_i = 1 km, **b** L_i = 2 km, **c** L_i = 3 km and **d** L_i = 4 km
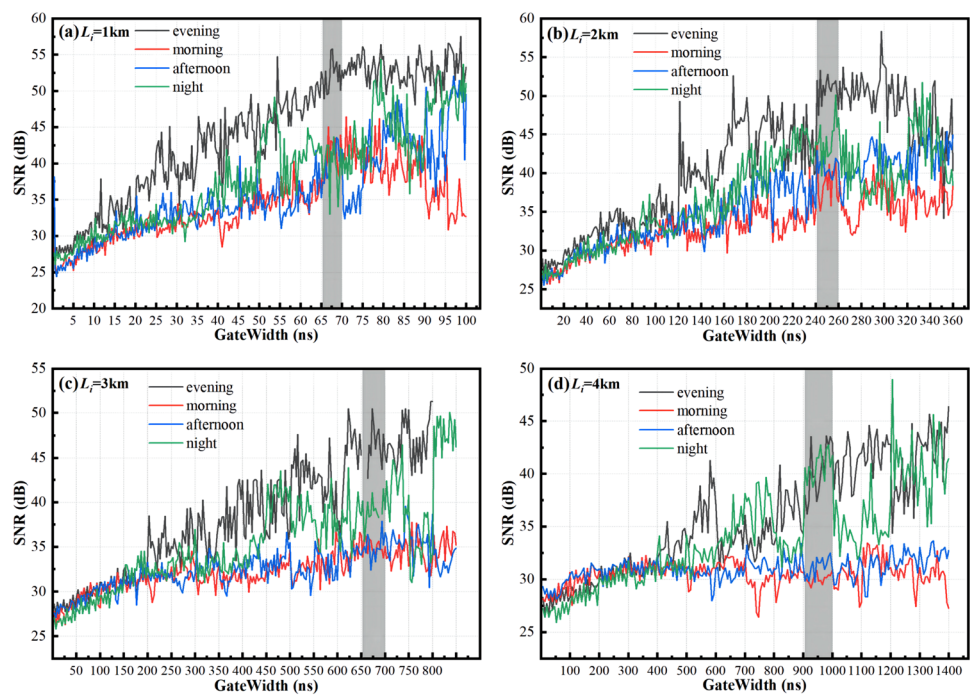
3. The green curve is detected in the night. Its SNR is higher than that of the morning and afternoon, considering the low background noise at night.

Therefore, detection at various times and distances adheres to the principle that the SNR of the spot image rises as the t_p increases, and it plateaus after reaching a certain point.

According to experiments, it can be concluded that in this DIM LiDAR detection system, When L_i = 1 km, 2 km, 3 km, and 4 km, t_p = 70 ns, 260 ns, 650 ns and 1us can be used as a more suitable gate width. The gray marked part in Fig. 8.

5 Conclusion

Through in-depth analysis of the principle of distance gating technology when using DIM LiDAR to detect turbulence, the relationship between gate width and detection distance is provided. The field experiment utilized the existing DIM LiDAR system in the laboratory. The results indicate that, at a constant detection distance, there is a gradual increase in the SNR of the image with increasing gate width, followed by a saturation point. The higher the SNR, the closer the inverted C_n^2 is to the ultrasonic anemometer. Meanwhile, if the SNR is similar, the inverted C_n^2 is similar. Therefore, through experiments, it was derived that the suitable gate widths for detecting 1 km, 2 km, 3 km, and 4 km in this system are 70ns, 260ns, 650ns, and

1us, respectively. The results of this study can be used for parameter optimization in detecting turbulence using DIM LiDAR, thereby achieving more accurate detection.

Declarations

Materials availability Not applicable.

Code availability Not applicable.

References

1. X.D. Guo Zhenhua, W. Shipeng, The influence of atmospheric turbulence on laser transmission. Laser Technol. **16**(2), 65–72 (1992)

2. Y. Haifeng, N. Xiaolong, C. Chunyi, Channel compensation based on pulse laser transmission in the atmosphere. J. Opt. **38**(1), 0101003 (2018)

3. D.L. Fried, Differential angle of arrival: theory, evaluation, and measurement feasibility. Radio Sci. **10**(1), 71–76 (1975)

4. A.H. Waldie, D.B. Soules, J.J. Drexler, F.D. Eaton, W.A. Peterson, J.R. Hines, A new high speed two-dimensional ccd atmospheric turbulence monitor, in: *Optical, Infrared, Millimeter Wave Propagation Engineering*, vol. 926 (SPIE, 1988), pp. 335–346

5. R.A. Johnston, N.J. Wooder, F.C. Reavell, M. Bernhardt, C. Dainty, Horizontal scintillation detection and ranging cn2 (z) estimation. Appl. Opt. **42**(18), 3451–3459 (2003)

6. R. Avila, E. Masciadri, J. Vernin, L. Sánchez, Generalized SCIDAR measurements at San Pedro Mártir. I. Turbulence profile statistics. Publ. Astronom. Soc. Pac. **116**(821), 682 (2004)

7. W. Caiyu, Numerical simulation and experimental analysis of atmospheric turbulence profiles detected by lidar. Master's thesis, University of Science and Technology of China (2021)

8. H. Zaihong, W. Yi, Z. Shouchuan, Development of turbulent profile lidar. Strong Laser Part. Beam **18**(10), 1602–1604 (2006)

9. S. Jian, Z. Xiaohui, G. Weilong, The impact of gating signals on image quality in range gated laser underwater imaging systems. Acta Opt. Sin. **29**(8), 2185–2190 (2009)

10. W.-l. Ge, L.-H. Hua, H.-W. Han, Analysis on the influences of range-gated underwater laser imaging system parameters on the signal to noise ratio. In: International symposium on photoelectronic detection and imaging 2013: laser sensing and imaging and applications, vol. 8905 (SPIE, 2013), pp. 129–137

11. Y. Xu, Design and accuracy study of selective laser imaging touch system. Master's thesis, Harbin Institute of Technology (2015)

12. W. Rui, The effect of laser range gated imaging gate width on image signal-to-noise ratio. China Opt. **8**(6), 951–956 (2015)

13. T. Xiaobo, Y. Wenjun, T. Wusheng, Simulation analysis of main parameter adjustment in range gated imaging. J. Weapon Equip. Eng. **37**(4), 74–80 (2016)

14. N. Qianqian, Y. Jiahao, L. Xiaolin, Design and study of time-resolved femtosecond laser-induced breakdown spectra. Spectrosc. Spectr. Anal. **43**(4), 1083–1087 (2023)